Polymer Testing 73 (2019) 439–446

Contents lists available at ScienceDirect

Polymer Testing

journal homepage: www.elsevier.com/locate/polytest

Experimental and theoretical investigation of heat transfer in platform bed during polymer extrusion based additive manufacturing

Darshan Ravoori, Christian Lowery, Hardikkumar Prajapati, Ankur Jain*

Mechanical and Aerospace Engineering Department, University of Texas at Arlington, Arlington, TX, USA

ARTICLE INFO

Keywords:
Additive manufacturing
Polymer extrusion
Heat transfer
Thermal diffusion
Infrared thermometry

ABSTRACT

Heat transfer plays a key role in polymer extrusion based additive manufacturing (AM) processes. Measurement and modeling of how temperature distribution on the platform bed changes with time during the dispensing of a polymer filament is of particular interest, as it determines the effectiveness of merging with neighboring filaments, and therefore, the properties of the built part. This paper reports infrared thermography based measurement of temperature field on the platform bed as a function of time during filament dispense and comparison with an analytical model based on moving heat source theory. Measurements identify two key heat transfer processes that influence temperature distribution on the bed. Data show that diffusion of thermal energy deposited on the bed with the filament and heat transfer from the hot nozzle tip both influence the temperature distribution on the bed. The relative contributions of these two sources of temperature rise on the bed are measured for different values of key process parameters. Measurement of temperature rise due to diffusion of thermal energy deposited on the bed is found to be in excellent agreement with an analytical model based on moving heat source theory. Evolution of the temperature field after completion of rastering of a line is measured. These data play a critical role in determining how effectively a filament merges with neighboring filaments. By identifying the key heat transfer processes that determine the temperature field on the platform bed, this work contributes towards thermal optimization of polymer-based additive manufacturing.

1. Introduction

Additive manufacturing (AM) is a broad class of manufacturing processes based on selective, layer-by-layer build up that offers significant design and manufacturing flexibility compared to traditional manufacturing approaches [1–4]. A number of AM processes are based on thermoplastic polymer materials such as Acrylonitile butadiene styrene (ABS), Polylactic acid (PLA), etc., wherein a polymer filament is heated to above its glass transition temperature in a heater block and then extruded through a nozzle tip on to a bed. Relative motion between the nozzle and bed facilitates rastering of the filament. Once deposited on the bed, polymer filaments cool down over time while merging with adjacent filaments. Polymer AM is relatively inexpensive and has been investigated widely for engineering and biomedical applications [5–9].

The process of merging of discrete polymer lines into each other to form the final part is at the core of the polymer AM process [2,10]. The nature and extent of such merging ultimately determines the properties of the final part such as Young's modulus, thermal conductivity, etc. [10–12]. Therefore, it is critical to understand how process parameters influence the filament bonding process. Clearly, heat transfer plays a critical role in this process. Heat transfer occurs from one filament to the other, from filaments into the bed and from filaments into the ambient [13,14]. These heat transfer processes determine the temperature history of the merging filaments. It is of interest, for example, to optimize the underlying heat transfer processes and enable the filaments to stay at a temperature greater than the glass transition temperature for as long as possible in order to facilitate effective merging of the filaments.

A few papers have carried out experimental measurements of heat transfer during the merging of polymer filaments on a bed. Note that the bed on which the filaments are deposited may comprise either previously deposited layers or, in the case of the first layer, the build plate on which the part is printed. Infrared thermography, a non-invasive temperature measurement technique, with extensive past work related to microelectronics and microelectromechanical systems (MEMS) [15–17] offers the capability of measuring the entire temperature field with good spatial and temporal resolution. Infrared thermography has been used for measuring temperature distribution on the bed as a function of depth [18], although these data have not been

* Corresponding author. 500 W First St, Rm 211, Arlington, TX, 76019, USA
E-mail address: jaina@uta.edu (A. Jain).

https://doi.org/10.1016/j.polymertesting.2018.11.025
Received 27 October 2018; Accepted 17 November 2018
Available online 22 November 2018
0142-9418/

Nomenclature

A	Extruder nozzle cross section area, m^2	T_0	Bed temperature, K
C_p	Heat capacity, J/kgK	T	Time, s
k	Thermal conductivity, W/mK	U_x	Nozzle speed in x direction, m/s
$\dot{m}$	Mass flow rate, kg/s	V	Filament speed, m/s
$\dot{q}$	Rate of energy deposition, W	x,y,z	Spatial coordinates, m
T	Temperature, K	α	Thermal diffusivity, m^2/s
T_n	Nozzle temperature, K	ρ	Density, kg/m^3
		ξ	Transformed coordinate, m

compared with theoretical models. Filament temperature distribution in the standoff region has also been measured using an infrared camera [19]. Process monitoring for fabricating thin wall composites has been reported using infrared thermometry [13], showing that temperature plays a key role in the degree of warping and cracking in the thin walls. Embedded micro-thermocouples have also been used for temperature measurement, although this approach only provides a local temperature measurement [20]. Post-process annealing has been investigated as a possible mechanism for improving filament-to-filament bonding, and therefore the overall strength [21] and thermal conductivity [22] of the final part. Heat transfer processes prior to filament deposition, including polymer melting and extrusion through the nozzle, as well as heat transfer in the standoff region between nozzle tip and bed have also been measured [19,23,24].

Theoretical and numerical analysis of heat transfer processes in polymer AM has also been presented in several papers. An analytical model based on principle of energy conservation in the deposited filament has been presented, although this model accounts for filament-to-bed heat transfer only through a convective heat transfer coefficient [25]. Heat transfer between filaments, and between filament and bed has been analyzed based on areas of contact, resulting in prediction of the quality of bonding [14]. Both lumped [20,21] and multi-dimensional [26] models are available. From a heat transfer perspective, the rastering of the filament on the platform bed can be described as a moving heat source [27]. This approach has been used extensively for thermal modeling of similar processes such as welding [28,29,30], but no application of moving heat source theory for polymer AM appears to exist.

Clearly, there is a need for systematic measurements and modeling for quantifying the heat transfer processes that influence temperature distribution in the layer being printed and in previously printed layers underneath, as this critically affects the extent and quality of bonding between adjacent filaments. Since the hot filament dispensed on the bed has greater energy due to its high temperature relative to the bed, it will clearly result in bed temperature rise once deposited. In addition, due to the short standoff gap between nozzle tip and bed, and the relatively high nozzle tip temperature, heat transfer from nozzle tip to bed in the form of thermal conduction and/or radiation may also be an important process in the dynamics of bed temperature as the nozzle tip rasters over the bed. A careful theoretical analysis of these phenomena, when combined with experimental measurement of the temperature field may help understand the fundamentals of heat transfer in polymer AM, and hence lead to design tools for engineering the thermal and mechanical properties of the built part.

This paper presents experimental measurement of temperature distribution on the bed using infrared thermography and comparison with a theoretical model based on moving heat source theory in a broad range of process parameters. Experiments without and with filament dispense from the hot nozzle tip quantify the contributions of thermal energy deposited with the filament and heat transfer from the hot nozzle tip on the bed temperature, showing that heat transfer from the nozzle tip plays a significant role in this process. Experimental data at a number of raster speeds and nozzle-to-bed gaps are found to be in good agreement with theoretical heat transfer models. Measurements of temperature decay in a filament after completion of the dispense process are also presented. These measurements and models offer previously unavailable insight into the process parameters that affect temperature distribution on the platform bed during polymer AM, which can be used for engineering the quality of bonding between adjacent filaments in polymer AM.

Section 2 describes the experimental setup for infrared thermography measurements. Theoretical model for temperature distribution

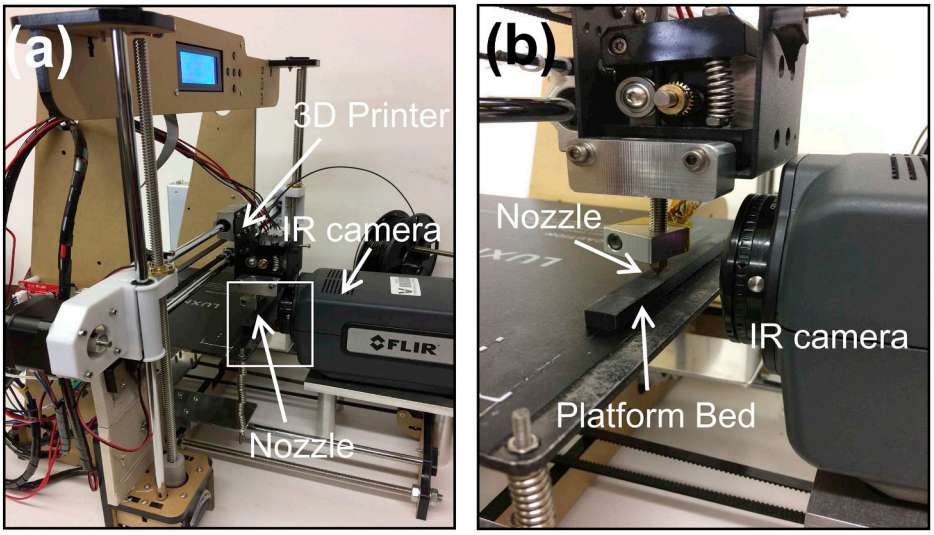

Fig. 1. (a) Picture of the experimental setup for infrared thermography during filament rastering process in polymer-based additive manufacturing (AM), showing various AM platform components and IR camera; (b) Zoom-in of the experimental setup.

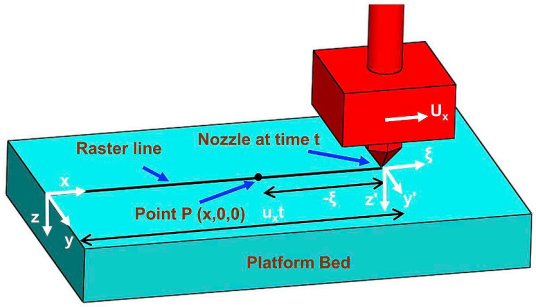

Fig. 2. Schematic of the filament rastering process, showing one-dimensional motion of the nozzle across the bed. The coordinate axes used in the analytical model are also shown for reference (Adapted from Ref. [28]).

on the bed due to a moving heat source is described in Section 3. Key results are presented and discussed in Section 4.

2. Experiments

Experiments are carried out to measure temperature distribution along the line of filament dispense on top of a bed as the nozzle traverses across the bed. The next two sub-sections describe the experimental setup and infrared camera calibration respectively.

2.1. Experimental setup for polymer extrusion and temperature measurement

All experiments are carried out on the open source Anet A8 3D printer platform. In contrast with other commercially available 3D printers, the Anet A8 platform facilitates the mounting of the IR camera within 4–7 cm of the nozzle path in order to capture infrared images along the raster line. In addition, this platform also facilitates changes in process parameters such as raster speed, bed temperature, etc. A 220 mm by 220 mm Aluminum platform is used. Filament is dispensed through a 0.4 mm brass nozzle heated by a 40W resistive heater connected to an aluminum heater block. Anet mainboard A1284 is used to control the stepper motors and power input to the heated bed as well as the nozzle heater.

Temperatures of the nozzle tip and platform bed are set at 205 °C and 60 °C respectively. In each experiment, a previously deposited Poly lactic acid (PLA) block serves as the bed on which a PLA filament is dispensed. In each case, a single line of filament is dispensed as the nozzle moves at fixed speed across the viewing field of the infrared camera. Raster speed is controlled via G-Code, which is processed using Simplify3D software for the specific 3D printer. The gap between PLA base and nozzle is controlled by varying the z axis parameter in the G-Code. Raster speed is confirmed through an independent measurement based on the length of filament dispensed in a fixed time interval. This calculation of the raster speed is found to be consistent with the speed set in the G-Code.

Temperature distribution in the entire field of view of the camera is captured in each experiment at a rate of 30 frames per second, following which, temperature data along the raster line are extracted.

Fig. 1(a) shows a picture of this experimental setup. A zoom-in image of the experiment is shown in Fig. 1(b).

2.2. Infrared camera calibration

While the infrared camera offers a convenient, non-invasive mechanism for temperature field measurement, a rigorous, pre-experiment calibration is essential to ensure accuracy. A thin part of thickness 0.4 mm printed from the same PLA material used in all other experiments is placed on a temperature-controlled Instec HCS622V stage. A FLIR A6703 3.0–5.0 μm InSb infrared camera is used. At multiple settings of the stage temperature, temperature of the top surface of the thin part is measured by a T-type thermocouple as well as the infrared camera. Temperature is allowed to stabilize over 20 min at each point prior to measurement.

3. Analytical modeling

From a heat transfer perspective, the process of rastering of the filament on the bed can be represented by a heat source moving along the raster line. Solutions for the temperature distribution for such moving heat source problems already exist [27,28] and have been applied for other engineering problems such as welding and laser cutting [29,30]. This section briefly summarizes the key results of this model and then applies it to the problem of determining temperature distribution in polymer dispense based additive manufacturing, with the primary goal of predicting temperature distribution on the surface of the bed, since this directly impacts the extent and quality of bonding between adjacent filaments.

Fig. 2 shows a schematic of the filament deposition process and subsequent thermal diffusion into the bed, which may comprise of already printed layers, or the underlying build plate on which the part is built. The filament is assumed to be deposited by a nozzle moving at a constant speed u_x along the x axis on the $z = 0$ face of the bed, which is assumed to be thermally semi-infinite. This assumption is justified by the short penetration depth expected within the short time duration in which a filament is deposited. Fig. 2 also shows a coordinate system attached to the moving nozzle, in which the coordinate ξ is given by $\xi = (x - u_x t)$. Mass of the filament deposited on the bed is assumed to be negligible compared to the bed mass, so that the only effect of filament dispense is the deposition of thermal energy $\dot{q}$ on the bed face, which then diffuses into the bed. $\dot{q}$ represents the rate at which thermal energy is deposited on the bed along with the filament material. This energy originates from the temperature of the deposited filament, the rate of deposition and heat capacity of the filament material as follows:

$$\dot{q} = \int_{T_0}^{T_n} \dot{m} C_p dT \tag{1}$$

where the mass flow rate $\dot{m} = \rho A V$ can be determined from the nozzle cross section area A, filament speed V and filament density ρ. Also note that C_p is the filament heat capacity, and T_n and T_0 represent the nozzle and initial bed temperatures respectively. Equation (1) includes latent energy associated with glass transition that usually occurs at a temperature between T_0 and T_n.

Assuming isotropic heat transfer in the bed, temperature-independent thermal conductivity k and thermal diffusivity α, and no internal heat generation in the bed, the governing energy conservation equation for temperature distribution in the bed $T(x,y,z,t)$ is given by

$$\frac{\partial^2 T}{\partial x^2} + \frac{\partial^2 T}{\partial y^2} + \frac{\partial^2 T}{\partial z^2} = \frac{1}{\alpha}\frac{dT}{dt} \tag{2}$$

Assuming a thermally semi-infinite bed, boundary conditions associated with equation (2) are.

$$\frac{\partial T}{\partial y} \to 0 \ \ as\ y \to \pm\infty \tag{3}$$

And.

$$\frac{\partial T}{\partial z} \to 0 \ \ as\ z \to \pm\infty \tag{4}$$

In addition, the total heat flux out of an infinitesimal sphere of radius r drawn around the dispensed filament must equal $\dot{q}$

$$\lim_{r\to 0}\left[-4\pi r^2 \cdot k \cdot \frac{\partial T}{\partial r}\right] = \dot{q} \tag{5}$$

where $r = \sqrt{(x - u_x t)^2 + y^2 + z^2}$ is the radial distance from the

filament location in the coordinate system attached to the moving nozzle.

Using coordinate system transformation, a solution for equations (2)–(5) has been shown to be [28].

$$T = T_o + \frac{\dot{q}}{2\pi kr} exp\left[-\frac{u_x(r+\xi)}{2\alpha}\right] \tag{6}$$

Complete details of the derivation of equation (6) may be found in Ref. [28].

In the case of filament rastering on the bed, the interest is specifically on temperature distribution on the top surface, $z = 0$. Also, along the line of filament dispense, the value of y is zero, as shown in Fig. 2. Therefore, along the raster line, equation (6) can be simplified to

$$T = T_o + \frac{\dot{q}}{2\pi k \cdot |x - u_x t|} exp\left[-\frac{u_x(|x - u_x t| + x - u_x t)}{2\alpha}\right] \tag{7}$$

This shows that at any given point *(x,0,0)* as shown in Fig. 2, prior to nozzle arrival, i.e. $t < \frac{x}{u_x}$, temperature is given by

$$T = T_o + \frac{\dot{q}}{2\pi k \cdot |x - u_x t|} exp\left(-\frac{u_x|x - u_x t|}{\alpha}\right) \tag{8}$$

And after the nozzle has passed over the point, temperature is given by.

$$T = T_o + \frac{\dot{q}}{2\pi k \cdot |x - u_x t|} \tag{9}$$

Note that $|x|$ refers to the absolute value of x. Equation (8) indicates a very slow rise in temperature when the nozzle is somewhat far during its approach towards the point, followed by a sharp exponential increase when the nozzle is close by. Afterwards, once the nozzle has passed over the point, equation (9) predicts a gradual reduction in temperature.

In addition to the bed surface, equation (6) is also capable of predicting temperature distribution as a function of depth inside the bed. As an illustration of this, Fig. 3 plots temperature distribution in a cross-section of the bed at three different times as the nozzle tip rasters across the top of the bed at 3.2 mm/s speed. Fig. 3 shows very high temperature near the nozzle tip location in each case and a rapid reduction in temperature before and after. The heat-affected zone moves along with the nozzle tip as it traverses across the bed, with some residual temperature rise downstream of the nozzle. Most of the temperature rise is limited to a shallow depth in the bed comprising just a few previously built layers, which is consistent with experimental observations from past papers [18,26], and occurs due to the short thermal penetration depth in the small time over which a filament is deposited. Note that Fig. 3 only accounts for temperature rise due to thermal energy deposited on the bed. Temperature rise may also occur due to other effects, such as heat transfer from the hot nozzle tip, which is further discussed in Section 4.

4. Results and discussion

4.1. Calibration of infrared thermography

Fig. 4 shows a calibration of the infrared camera used in this work for temperature measurement. As described in section 2, temperature of the top surface of a printed PLA sample is measured both through a T-type thermocouple in direct contact with the surface as well as the infrared camera at a number of temperatures in the 75 °C–210 °C range of interest. A value of 0.92 is used for the emissivity of PLA in the wavelength range detected by the infrared camera. Fig. 4 plots temperature measured by the infrared camera against thermocouple measurement at a number of temperature points, showing good agreement over the entire temperature range of interest. All points lie close to the ideal 45° line. This establishes the accuracy of the infrared thermometry approach for temperature measurement utilized in all measurements in this work.

4.2. Effect of raster speed on temperature distribution

A number of experiments are carried out to measure temperature distribution on the platform bed along the raster line. In each case, the temperature field is recorded as a function of time at a rate of 30 frames per second, so that transient variations in the temperature field can be captured. At a fixed point on the line, as the nozzle tip approaches the point, temperature is expected to go up. When the nozzle is directly above the point of interest, the temperature is expected to be the highest, and then decay as the nozzle moves away. The nature of temperature rise prior to nozzle arrival as well as decay afterwards are both very important for understanding filament-to-filament merging and bonding. Infrared thermography of the filament dispensing process is carried out in a number of process conditions. As an example, Fig. 5(a)-(c) show infrared thermographs captured at three different times for a dispense process at 2.7 mm/s raster speed. In these images, the nozzle tip moves from left to right. Temperature distribution along the raster line can be clearly seen in these images. The peak temperature occurs directly under the nozzle tip and moves from left to right along with the nozzle tip. In each case, temperature distribution as a function of space and time can be extracted quantitatively from the infrared thermographs such as Fig. 5(a)-(c).

To further illustrate the temperature measurement approach, the effect of raster speed on temperature distribution is examined. Fig. 6(a) plots temperature as a function of time at a fixed point *A* along the raster line for three different raster speeds. These measurements show that the peak temperature reached at point *A* is invariant with raster speed. However, as expected, the time at which the peak temperature occurs changes with raster speed, occurring later at lower raster speeds. At each raster speed, temperature rises slowly as the filament front approaches the point of interest. An inflexion in the measured temperature is observed when the filament front is around 3.5 mm away from the point of interest, leading to very sharp increase in temperature until the peak corresponding to the arrival of the nozzle tip directly above the point of interest. While the measured temperature is expected

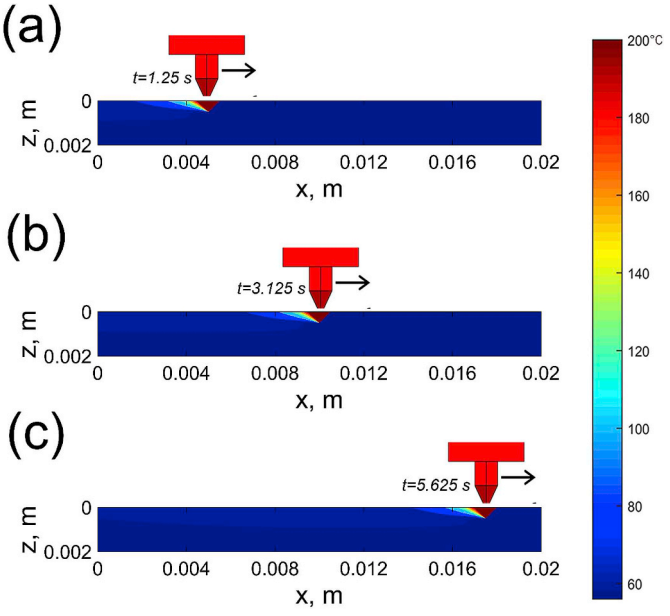

Fig. 3. Colorplot of temperature distribution in the platform bed during the rastering of the nozzle at a 3.2 mm/s speed, based on analytical model for diffusion of thermal energy deposited by the hot filament. Colorplots are shown at three successive times.

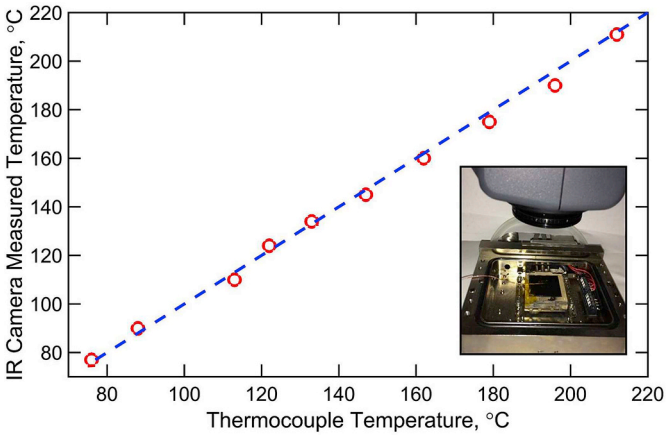

Fig. 4. Comparison of temperature of the top surface of a PLA block measured by infrared camera with direct thermocouple measurement over the temperature range of interest. An emissivity value of 0.92 for the infrared camera results in excellent agreement between the two. Inset in the figure shows a picture of the experimental setup for calibration.

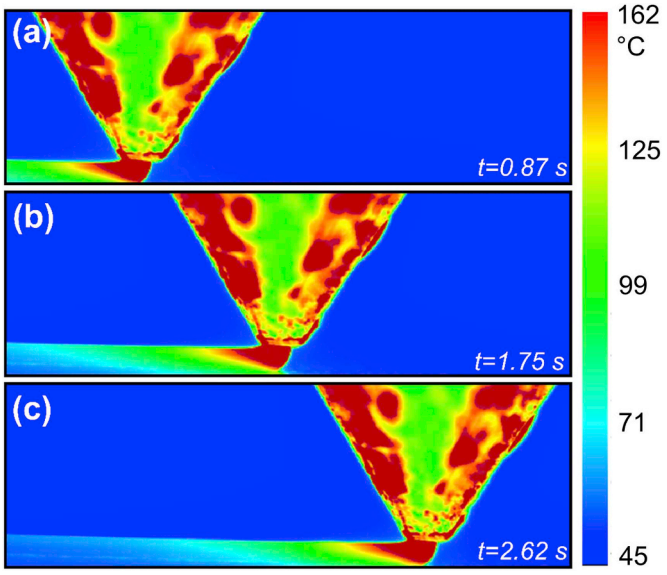

Fig. 5. Infrared thermographs obtained at three different times for rastering of a single line wherein the nozzle moves from left to right at 2.7 mm/s speed.

to rise as the nozzle tip approaches, the inflexion in temperature, observed consistently in all experiments indicates that temperature rise at the point of interest may be influenced by another heat source in addition to diffusion of thermal energy deposited by the dispensed filament.

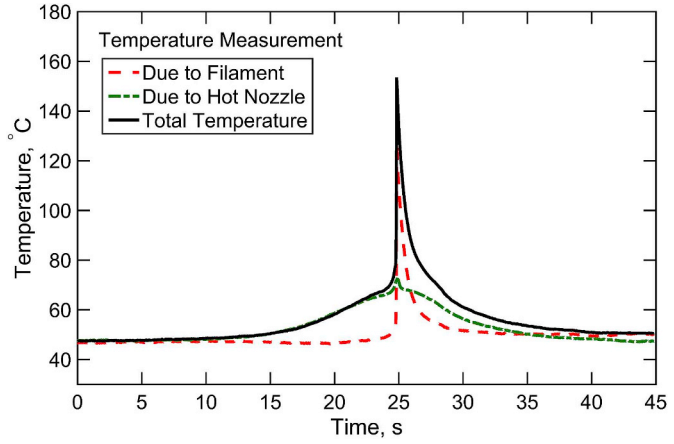

Fig. 7. Plot of the contributions from energy deposition by hot filament dispense and thermal conduction from hot nozzle tip towards temperature at a point on the platform bed. Sum total of the two contributions is also shown.

These measurements are repeated for two additional points – *B* and *C* – as shown in the insets of Fig. 6(b) and (c). Points *B* and *C* are further downstream of point *A*. Fig. 6(b) and (c) show, as expected that the time at which temperature peak occurs at these points is later than in the case of point *A*. The shapes of temperature curves, including the inflexion point as well as the peak temperature value in Fig. 6(b) and (c) are all consistent with Fig. 6(a). Peak temperature is nearly the same at each point, which is consistent with the semi-infinite nature of the bed in the short time duration of these experiments.

4.3. Contributions of filament dispensing and hot nozzle tip towards temperature rise

As discussed in Section 3, diffusion of thermal energy deposited along with the dispensing filament into the bed causes temperature rise. In addition, thermal conduction from the nozzle tip may also play a role due to the close proximity of the nozzle tip.

In order to investigate these factors that affect temperature rise and its variation with time, temperature at a specific point *A* along the filament dispense line is measured at a raster speed of 2.7 mm/s. These measurements, carried out with and without filament dispensing out of the nozzle tip, are plotted in Fig. 7. The nozzle tip is at 205 °C in both experiments and the gap between nozzle tip and bed is 0.4 mm. Clearly, data from the experiment without filament dispense corresponds to the contribution of thermal conduction from the hot nozzle tip alone, since hot filament is not being dispensed on the bed. On the other hand, data from the experiment with filament dispense is the sum total of contributions from both thermal energy deposited along with filament and heat transfer from the hot nozzle tip. Due to the linearity of heat transfer in this problem, contributions from these two sources are expected to add up linearly. Therefore, the difference between

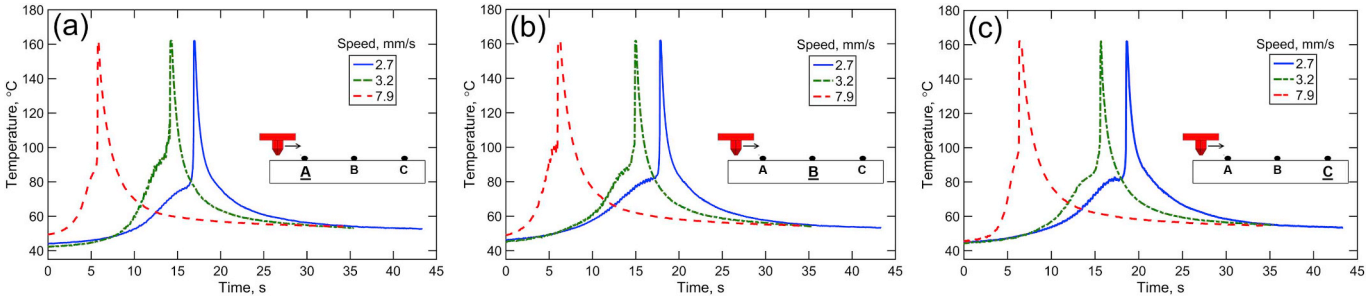

Fig. 6. Measured temperature as a function of time at a fixed location along the raster line for three different raster speeds. (a)–(c) present these data for three distinct points *A*, *B* and *C* along the raster line as shown in the inset schematics.

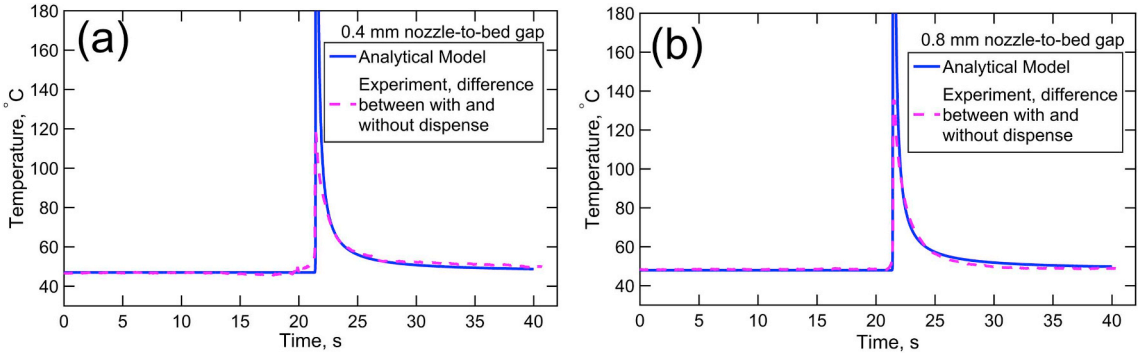

Fig. 8. Comparison of the effect of heat transfer from hot nozzle tip with prediction from moving heat source theory for 0.4 mm and 0.8 mm nozzle-to-bed gap.

experimental data in the two cases represents the effect of thermal energy deposited along with the filament, which is also plotted in Fig. 7. In this manner, these two experiments clearly separate out the contributions of both sources of temperature rise. Fig. 7 shows that thermal energy deposited along with the filament has negligible effect on temperature rise on the bed until the nozzle is very close to the point of interest, beyond which, the temperature rises very rapidly and then decays away once the nozzle has passed. This behavior is representative of typical predictions from moving heat source theory discussed in section 3. On the other hand, temperature rise due to heat transfer from the hot nozzle increases faster during approach of the nozzle towards the point of interest, but does not peak as dramatically as the contribution from the hot filament dispense. Temperature rise due to heat transfer from the hot nozzle occurs primarily due to thermal conduction and radiation across the small gap between nozzle and bed.

The large size of the hot nozzle compared to the filament diameter explains why temperature rise due to the hot nozzle is spread out over a larger time interval compared to temperature rise due to the filament. The experiment without filament dispense also explains the inflexion point observed in Fig. 6 – it occurs due to the arrival of the hot nozzle block above the point of interest before the actual dispensing of the filament at that point.

To further validate this, the difference between experimental data with and without filament dispense, which represents the temperature rise only due to thermal energy deposited along with the filament is compared against predictions from the moving heat source theory, which accounts for heat diffusion from the dispensed filament into the bed. Fig. 8(a) shows very good agreement between the two. As discussed in section 3, due to the presence of a singularity at $t = x/u_x$, moving heat sources theory predicts infinite temperature when the nozzle tip is precisely at the point of interest. This may restrict comparison of theoretical predictions with experimental at exactly that time. However, it accurately tracks measured temperature both before and after nozzle arrival, as shown in Fig. 8. In particular, the decay of temperature at the point of interest after the nozzle has passed is important for determining the quality of bonding at that point with neighboring filaments. The model correctly captures this transient, as shown in Fig. 8. The contribution from the dispensed filament does not lead to significant temperature rise until the nozzle tip is very close to the point of interest, at which time, temperature rises extremely fast. This is consistent with moving heat source theory that predicts flat temperature at early times followed by a sharp increase in temperature just prior to nozzle arrival at the point of interest.

Data presented in Figs. 7 and 8 not only identify and quantify the relative contributions of the two sources of temperature rise, but also validate the measurements through good agreement with an analytical model. The key role played by heat transfer from the hot nozzle through the standoff gap is particularly interesting and not necessarily intuitive.

The influence of heat transfer from the nozzle tip on temperature rise in the bed is investigated further through experiments at two different values of the gap between the nozzle tip and bed. Fig. 9 plots the temperature component at a fixed point due to heat transfer from the hot nozzle tip, determined from experiments without filament dispense at two different gaps. These data clearly show a reduction in temperature rise due to the hot nozzle when the gap is increased, further confirming the important role of heat transfer from the nozzle tip. Heat transfer between the two bodies is expected to reduce with increasing gap, as shown in these experimental data. The small bumps in the curves in Fig. 9 correspond to the time of arrival of the nozzle body above the point of interest. Further, Fig. 8(b) plots temperature rise due to thermal energy deposited along with filament for 0.8 mm gap and

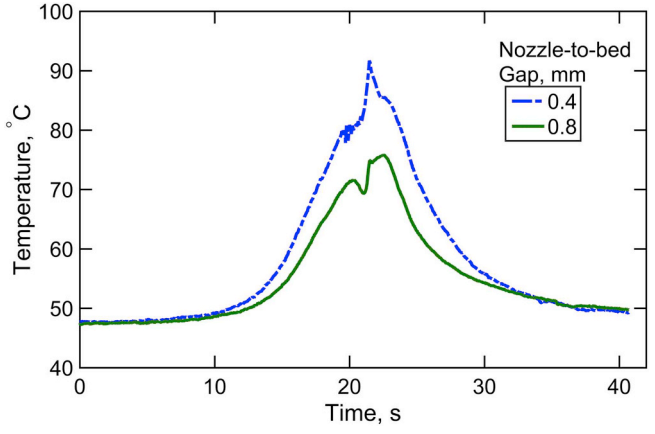

Fig. 9. Temperature due to thermal conduction from hot nozzle tip at a point on the raster line as a function of time for two different nozzle-to-bed gaps.

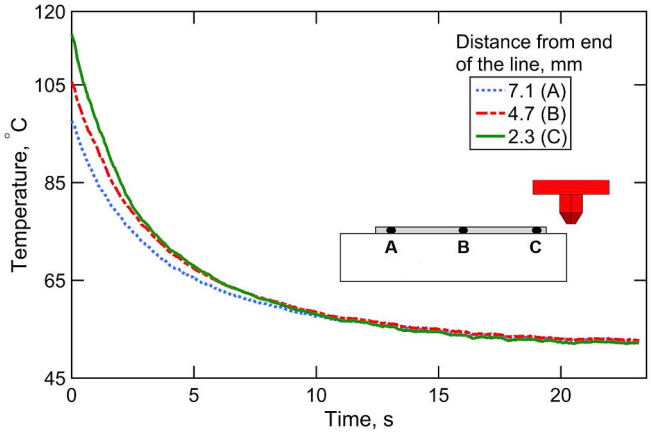

Fig. 10. Temperature decay as a function of time at three different points on the raster line after completion of the raster process. Locations of the points are shown in the inset schematic.

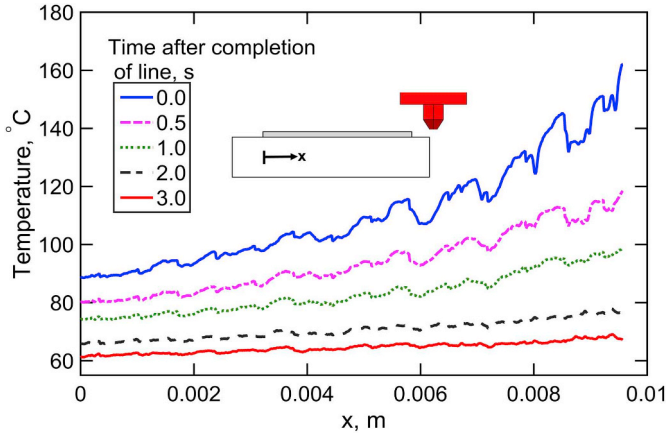

Fig. 11. Temperature of the entire raster line at multiple times after completion of the raster process.

compares against predictions from moving heat source theory. Similar to the 0.4 mm gap case shown in Fig. 8(a), there is good agreement in this case as well, further validating the experimental approach for understanding the contributions from the two sources on temperature rise in the platform bed and the role of the nozzle-to-bed gap on temperature rise.

4.4. Temperature decay in the filament after completion of dispense process

In addition to understanding temperature rise during the process of dispensing a filament line, the process of temperature decay in the line after completion of the dispense process is also important. For example, once a line has been dispensed, the nozzle tip typically moves over and dispenses the adjacent filament line. Merging of the two adjacent lines is critical for ensuring good mechanical strength of the built part. This process is driven primarily by the temperature history of the two merging filaments that must be kept at above glass transition temperature for as long as possible. In light of this, measurements are carried out to quantify the nature of temperature decay in the filament line after completion of the rastering process. Fig. 10 plots temperature as a function of time at three different points *A*, *B* and *C* on the filament line after completion of the filament dispense process. In this case, the line is printed from left to right at 3.2 mm/s speed, and point *C* is closest to the end point of the line, as shown in the inset in Fig. 10. Experimental data show that point *C* is initially the hottest among the three points considered. Temperature at each point decays smoothly and becomes uniform after about 8 s. Fig. 11 plots the entire temperature distribution along the filament line at multiple times. As expected, Fig. 11 shows an asymmetry in the temperature distribution at $t = 0$ s, since the far end of the line has been dispensed more recently than the end near $x = 0$. As the line cools down, temperature reduces everywhere along the line, while also becoming more thermally uniform. Quantitative measurement of temperature evolution along the line shown in Fig. 11 is critical because temperature at any point along the line influences the extent of bonding with the adjacent line, which is usually printed immediately afterwards while the first line is thermally decaying. Curves in Figs. 10 and 11 may be useful for optimizing the process parameters in order to ensure better and spatially uniform merging between filaments.

5. Conclusions

This work investigates heat transfer on the platform bed during filament deposition in polymer extrusion additive manufacturing. Quantification of temperature rise due to two distinct heat transfer mechanisms offers key insights into the nature of heat transfer in this process. Good agreement between experimental data and theoretical model over a broad range of parameters is demonstrated. Experimental methods and data from this work may be used for optimizing and improving polymer AM processes by ensuring good filament-to-filament bonding, and hence, good ultimate properties of the built part. For example, based on results from this work, process parameters could be manipulated in order to obtain desired filament-to-filament bonding. When optimized carefully, this may lead to parts with novel, spatially varying orthotropic properties. Further, a good understanding of heat transfer during polymer AM processes can also be used for printing parts with novel, multifunctional properties, which is particularly helpful in applications that call for multi-functional components.

References

[1] W.E. Frazier, Metal additive manufacturing: a review, J. Mater. Eng. Perform. 23 (2014) 1917–1928.
[2] J.P. Kruth, M.C. Leu, T. Nakagawa, Progress in additive manufacturing and rapid prototyping, CIRP Ann. - Manuf. Technol. 2 (1998) 525–540.
[3] P. Vojislav, V.H.G. Juan, J.F. Olga, D.G. Javier, R.B. P Jose, P.G. Luis, Additive layered manufacturing: sectors of industrial application shown through case studies, Int. J. Prod. Res. 49 (2010) 1061–1079.
[4] D.T. Pham, R.S. Gault, A comparison of rapid prototyping technologies, Int. J. Mach. Tool Manufact. 38 (1998) 1257–1287.
[5] N. Guo, M.C. Leu, Additive manufacturing: technology, applications and research needs, Front. Mech. Eng. 8 (2013) 215–243.
[6] H.J. Timothy, H.L. A Ola, Overview of current additive manufacturing technologies and selected applications, Sci. Prog. 95 (2012) 255–282.
[7] I. Zein, D.W. Hutmacher, K.C. Tan, S.H. Teoh, Fused deposition modeling of novel scaffold architectures for tissue engineering applications, Biomaterials 4 (2000) 1169–1185.
[8] S. Bose, S. Vahabzadeh, A. Bandyopadhyay, Bone tissue engineering using 3D printing, Mater. Today 12 (2013) 496–504.
[9] J.W. Stansbury, M.J. Idacavagec, 3D printing with polymers: challenges among expanding options and opportunities, Dent. Mater. 32 (2016) 54–64.
[10] D. Ravoori, L. Alba, H. Prajapati, A. Jain, Investigation of process-structure-property relationships in polymer extrusion based additive manufacturing through in situ high speed imaging and thermal conductivity measurements, Additive Manufacturing 23 (2018) 132–139.
[11] S. Ahn, M. Montero, D. Odell, S. Roundy, P.K. Wright, Anisotropic material properties of fused deposition modeling ABS, Rapid Prototyp. J. 8 (2002) 248–257.
[12] B.M. Tymrak, M. Kreiger, J.M. Pearce, Mechanical properties of components fabricated with open-source 3-D printers under realistic environmental conditions, Mater. Des. 58 (2014) 242–246.
[13] B.G. Compton, B.K. Post, C.E. Duty, L. Love, V. Kunc, Thermal analysis of additive manufacturing of large-scale thermoplastic polymer composites, Additive Manufacturing 17 (2017) 77–86.
[14] S.F. Costa, F.M. Duarte, J.A. Covas, Estimation of filament temperature and adhesion development in fused deposition techniques, J. Mater. Process. Technol. 245 (2017) 167–179.
[15] D. Anthony, D. Wong, D. Wetz, A. Jain, Non-invasive measurement of internal temperature of a cylindrical Li-ion cell during high-rate discharge, Int. J. Heat Mass Tran. 111 (2017) 223–231.
[16] L. Dupont, Y. Avenas, P. Jeannin, Comparison of junction temperature evaluations in a power IGBT module using an IR camera and three thermosensitive electrical parameters, Int. J. Heat Mass Tran. 49 (2013) 1599–1608.
[17] H.F. Hamann, A. Weger, J.A. Lacey, Z. Hu, P. Bose, E. Cohen, J. Wakil, Hotspot-limited microprocessors: direct temperature and power distribution measurements, IEEE J. Solid State Circ. 42 (2007) 56–65.
[18] J.E. Seppala, K.D. Migler, Infrared thermography of welding zones produced by polymer extrusion additive manufacturing, Additive Manufacturing 12 (2016) 71–76.
[19] H. Prajapati, D. Ravoori, A. Jain, Measurement and modeling of filament temperature distribution in the standoff gap between nozzle and bed in polymer-based additive manufacturing, Additive Manufacturing 24 (2018) 224–231.
[20] Q. Sun, G.M. Rizvi, C.T. Bellehumeur, P. Gu, Effect of processing conditions on the bonding quality of FDM polymer filaments, J. Manuf. Process. 14 (2008) 72–80.
[21] C. Bellehumeur, L. Li, Q. Sun, P. Gu, Modeling of bond formation between polymer filaments in the fused deposition modeling process, J. Manuf. Process. 6 (2004) 170–178.
[22] J. Go, S.N. Schiffres, A.G. Stevens, A.J. Hart, Rate limits of additive manufacturing by fused filament fabrication and guidelines for high-throughput system design, Additive Manufacturing 16 (2017) 1–11.
[23] M.E. Mackay, Z.R. Swain, C.R. Banbury, The performance of the hot end in a plasticating 3D printer, J. Rheol. 61 (2017) 229–236.
[24] C. Bellehumeur, L. Li, Q. Sun, P. Gu, Modeling of bond formation between polymer filaments in the fused deposition modeling process, J. Manuf. Process. 6 (2004) 170–178.
[25] A. D'Amico, A.M. Peterson, An adaptable FEA simulation of material extrusion additive manufacturing heat transfer in 3D, Additive Manufaturing 21 (2018) 422–430.

[26] N. Özışık, Heat Conduction, third ed., John Wiley & Sons, 2012.
[27] E. Kannatey-Asibu Jr., Principles of Laser Materials Processing, first ed., John Wiley & Sons, 2009.
[28] J. Mazumder, W.M. Steen, Heat transfer model for cw laser material processing, J. Appl. Phys. 51 (1980) 941–947.
[29] X. He, P.W. Fuerschbach, T. Debroy, Heat transfer and fluid flow during laser spot welding of 304 stainless steel, J. Phys. D Appl. Phys. 36 (2003) 1388–1398.
[30] H. Prajapati, D. Chalise, D. Ravoori, R.M. Taylor, A. Jain, Improvement in build-direction thermal conductivity in extrusion-based polymer additive manufacturing through thermal annealing, Unpubl. Results (2018).